

# Knit Happens: Designing the Mechanics of Machine Knitting

Cosima du Pasquier<sup>1,\*</sup>, Sehui Jeong<sup>1,\*</sup>, Pan Liu<sup>3</sup>, Susan Williams<sup>2</sup>,  
Allison M. Okamura<sup>1</sup>, Skylar Tibbitts<sup>2</sup>, Tian Chen<sup>3</sup>

**Abstract**—Knit fabrics are durable and tough while sufficiently flexible to conform to curved substrates like the human body. Advances in industrial knitting enable unprecedented control over the pattern design and functionality of next generation knit fabrics. However, the ability to leverage this granular control to predict and tune the mechanical behavior of fabrics remains limited due to their complex microstructure. This study establishes a comprehensive experimental and numerical framework to characterize and model the mechanical properties of knitted fabrics. The integration of experiments, simulation, and strain energy-based homogenization demonstrates how stitch length, pattern, and yarn material govern the anisotropic mechanical response of knitted fabrics. These parameters are quantitatively linked to key material properties, like stiffness and anisotropy. The framework is extended to heterogeneous knits to reflect the makeup of real-world textiles. Material transitions are found to have minimal impact on the fabric’s overall mechanical response, so heterogeneous fabrics can be modeled as patchworks of homogeneous samples. The framework is implemented in the design of the first industrially knit sleeve explicitly optimized for both fit and function. This work bridges the gap between computational modeling and scalable manufacturing, unlocking new possibilities for wearable devices, assistive textiles, and functional applications.

## KEYWORDS

Mechanics of Knits | Variable Stiffness Knitting | Multi-Scale Modeling | Entangled microstructures | Optimized Wearables

## INTRODUCTION

Knit fabrics have been used for millennia, valued for their mechanical robustness, ease of manufacturing, and expansive design space. As with other highly entangled material architectures, a knit’s appearance, texture, and mechanical properties are predominately govern by its microstructure [1]–[5]. Knitting is essentially an additive manufacturing process: yarns, spun from fibers, are interlocked in periodic patterns to form the fabric [6]. The friction and sliding between stitches allow knits to endure repeated large stretches, multiple washing and drying cycles, and harsh environmental conditions while maintaining durability over decades of use without the need for adhesives or additives [7]. While knitting as

a technique to produce textiles through the interlace of yarn loops have remained largely unchanged, industrialization has revolutionized the speed of production and the complexity of the resulting textiles in terms of material, heterogeneity and stitch density [8], [9].

Industrial knitting machines and computer-aided design tools have enabled unprecedented control and complexity of the manufacturing process and of the design space [10]. This in turn highlights the potential for research and innovation of modern knits beyond the fashion industry [11]. Unlike other fabrication methods, knitting offers a unique synergy between mechanics research and scalable manufacturing [11]. The same equipment used for development is utilized in production, reducing the need for process translation and enabling quick transitions from concept to final product. Designers have the ability to not only program the movement and action of every stitch, but also precisely control the timing of these actions. However, the advanced capabilities of industrial knitting are often underutilized due to our limited understanding of the mechanics of knits.

Accurate modeling of the mechanics of knits is challenging because their complex microstructure is based on the many interlocking and sliding elements (Fig. 1A) [12]–[17]. This is true for even the simplest homogeneous knits, and significantly more so with real-world fabrics that may be constructed from multiple layers of knits with heterogeneous patterns [13]. The two primary approaches for computational knit modeling aim to represent either their qualitative or quantitative behaviors. The qualitative approach emphasizes capturing the accurate kinematics and animation of knit fabric such as draping and clothing through homogenization [1], [6], [18]–[21], using tools such as CLO3D [22]. The quantitative approach aims to capture the physical mechanics at the different knit hierarchies from clasps with deformable silicone yarns [23]–[25] to loose knits with isotropic yarns, such as monofilament synthetic yarn and shape memory alloy [26], [27]. Multiscale modeling using homogenization can also be applied for physics-based methods [16], [28], [29].

In this work, we leverage advances in both approaches and demonstrate a mechanistic understanding of industrial knit fabrics through numerical modeling and precision experiments. We begin by homogenizing the anisotropic mechanical behavior of the different types of yarns. We then incorporate the yarn mechanics in a finite element-based (FE) volumetric model of representative knit stitches (Fig. 1A). We experimentally validate this model through a parametric study, where we explore isolated knit variations by fabricat-

This work was supported in part by NSF Grants #2301355, #2301356, and #2301357, as well as the Robert M. and Mary Haythornthwaite Foundation.

<sup>1</sup>Collaborative Haptics and Robotics in Medicine Lab (CHARM), Dept. of Mechanical Engineering, Stanford University, Stanford, CA 94305, USA. Email: cosimad@stanford.edu

<sup>2</sup>Self-Assembly Lab, Dept. of Architecture, Massachusetts Institute of Technology (MIT), Cambridge, MA 02139, USA.

<sup>3</sup>Architected Intelligent Matter Laboratory, Dept. of Mechanical and Aerospace Engineering, University of Houston, Houston, TX 77204, USA. Email: tianchen@uh.edu

\* CDP and SJ contributed equally to this work

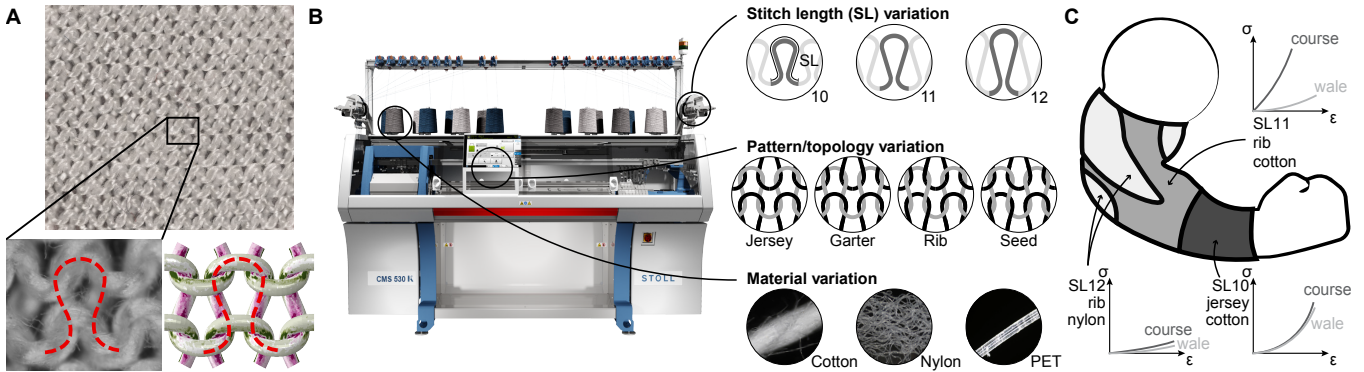


Fig. 1: Principles of knitted fabrics. A. An industrial knitting machine produced knit fabric. Knit fabrics feature a hierarchical microstructure starting from bundling of fibers which are then intertwined to form yarns. By geometrically reconstructing this pattern, we can build a volumetric FE model of a representative unit. B. An industrial knitting machine can vary yarn material, stitch length, and pattern/topology. Multiple yarn spools are available. Stitch length is controlled by varying the tension of the yarn. With basic knit patterns, 2 by 2 stitch with purl (P) or knit (K) form a basic periodic unit. These parameters can be changed within single fabrics. C. We leverage this unique capability to demonstrate wearable devices that cannot be feasibly fabricated with homogeneous knitting.

ing, pre-processing, and testing homogeneous fabrics with different stitch lengths, knit patterns, and yarn materials (Fig. 1B). Armed with both experimental and numerical results, we abstract the behavior of homogeneous fabrics using a simplified strain energy model that can be used in commercial FE tools to define the relationship between knit parameters and mechanical properties. Having quantified the effects of knit variations, we extend our framework to capture the mechanical response of knit transitions between variations. Finally, we design a heterogeneous knit sleeve that adapts to significant shape changes along the arm to provide constant pressure (Fig. 1C). Building on previous work, we employ homogenization methods to abstract microscopic behavior, enabling an efficient approach that can model both simple, homogeneous swatches and complex, real-world heterogeneous swatches, and ultimately facilitate the modeling and optimization of advanced functional garments.

#### MECHANICS OF YARNS.

Before modeling the behavior of knits, we start by characterizing the mechanical behavior of different types of yarns. We choose three types of yarns that are commonly used with knitting machines. Cotton is a 2-ply spun cellulose yarn with a mercerized finish. It consists of short staple natural fibers. Nylon is a synthetic extruded filament with high stretch. This stretchability arises from the many kinked continuous synthetic fibers running from end to end. Polyethylene terephthalate or PET is a stiff monofilament similar to fishing line.

Observing that the yarns behave differently in longitudinal and radial directions, we characterize this anisotropy experimentally [30]. The yarns are tensioned lengthwise, and compressed transversely as shown in Fig. 2. (Experiment setup based on Singal et al. [6]; see SI Section 2.) Nylon and cotton behave with transverse isotropy, where the cross-section is more compliant by four orders of magnitude than

the length direction due to the internal voids created by the fiber bundles (Fig. 2). PET, a monofilament, is isotropic.

In physical knit specimens, the diameter of a yarn in the knit can differ significantly from that of a free-standing yarn due to the tension applied during knitting. Therefore, we measure the diameter of the yarn at rest  $d_0$  and the diameter of the same type of yarn once knitted  $d_k$ . By comparing these measurements, we estimate the tension in the yarn within the knit fabric. The compression tests are conducted on pre-tensioned yarns. Using this experimental data, we homogenize the behavior of individual fibers and numerically model yarns in a knit as a solid curved rod.

#### MECHANICS OF HOMOGENEOUS KNIT FABRIC

A typical industrial knit fabric consists of different homogeneous knit units, each defined by varying knit parameters to provide target mechanical behaviors such as stiffness and stretchability. We begin by characterizing the behavior of these homogeneous knit units. To establish an experimental protocol that can be approximated in numerical modeling, we conduct a series of preliminary tests to identify key factors influencing a knit's mechanical response. These include: cyclic loading, washing and drying, viscoelasticity, and rupture. The preliminary test results are included in SI Section 5.

In these preliminary tests, we apply an equibiaxial strain of 10% to cotton specimens at a rate of 0.1 mm/s. The stress-strain curve of the fabric shows significant dependence on the maximum displacement previously experienced (SI Fig. S7). Subsequent loading to the same displacement exhibits considerable softening and reduced energy dissipation [31]. After washing and drying, the initial behavior is partially recovered, where subsequent testing shows the same softening behavior. Viscoelasticity does not have a significant effect when the displacement rate is varied from 0.1 to 0.4. Premature rupture was observed at the corners for

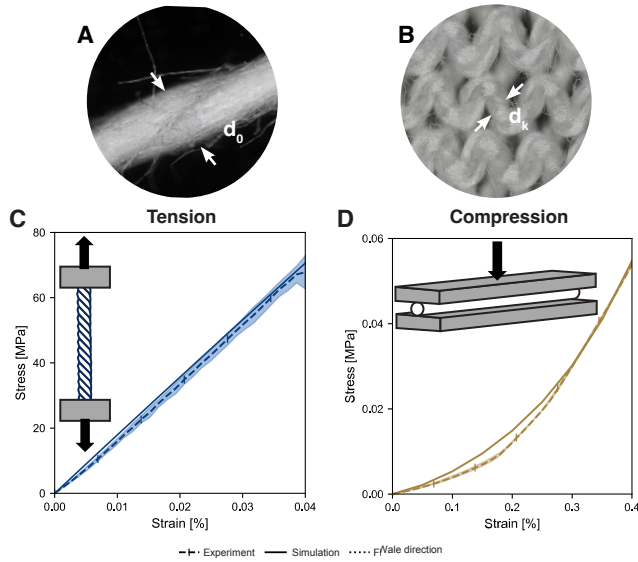


Fig. 2: Yarn testing methodology; microscopy images of cotton A. yarn and B. knit fabric sample; illustration of test procedure and results for cotton yarn testing in C. tension and D. compression.

square specimens. Therefore a cruciform geometry is used in subsequent experiments. The details of the tests can be found in SI Section 3.

We experimentally and numerically investigate the influence of two critical manufacturing parameters in knitting in addition to yarn materials. First, stitch length, dictated by the tension during knitting, directly affects the density of the fabric and its mechanical behavior. We consider three distinct stitch lengths (SL): loose, tight, and very tight (Fig. 1B). Physically, they range between settings of 10, 11, and 12, which are equivalent to stitch arc lengths of 3.89 mm, 4.71 mm, and 5.92 mm in Jersey, respectively. These lengths are machine and pattern dependent. Second, knitting patterns emerge from specific arrangements of knits and purls. Knits are pulled towards the face of the fabric, while purls are pulled towards the back. We examine four basic knit structures: single knit Jersey, Garter, Rib, and Seed (Fig. 1B). A Jersey pattern uses identical, Garter alternates rows, Rib alternates columns, and Seed alternates both. Column alternations are in the course direction, which refers to rows of stitches formed by continuous yarn running horizontally. Row alternations are in the wale direction, which corresponds to columns of stitches aligned vertically (Fig. 1B). The sample preparation and testing procedures are in **Materials and Methods**.

#### Numerical modeling

Our FE model captures the mechanical behavior of knits with different stitch lengths, pattern and yarn material. The knit geometry and topology is defined using explicit parametric equation of the yarn centerline [32]. Instead of modeling individual fibers, the mechanical behavior of the yarns (discussed above) is homogenized as an isotropic (PET) or

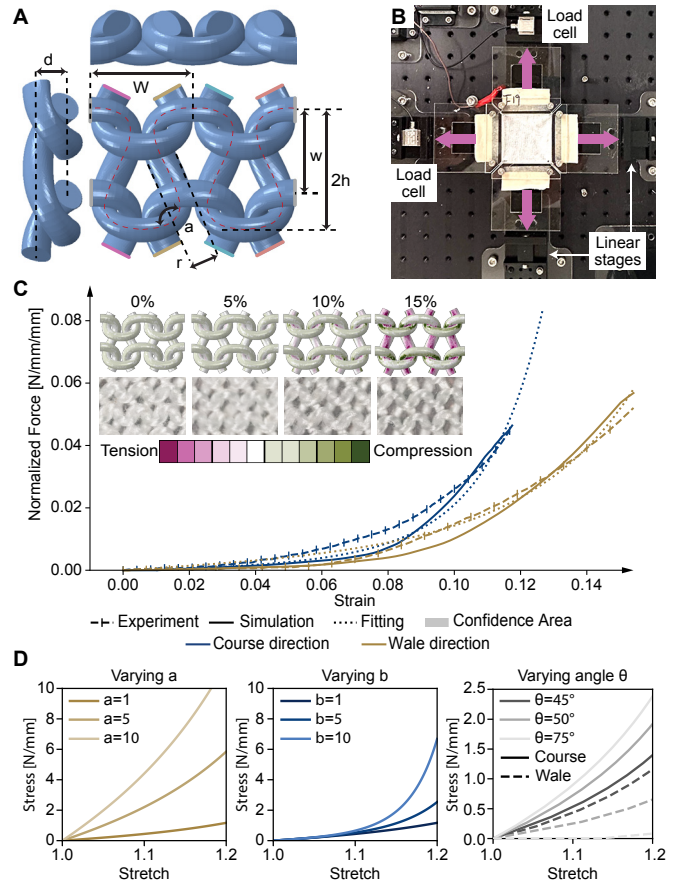


Fig. 3: Fabric swatch numerical and experimental methodology; A. Finite Element (FE) model showing the geometry of a 2 by 2 knit structure, the parameters defining the centerline, and color-coded boundaries that are tied to enforce periodicity; B. Biaxial experimental stage that imposes different biaxial strain states on the swatches; C. Normalized Force-Displacement plot of a benchmark knit sample in both X (course) and Y (wale) directions resulting from the FE simulation, reduced-order model, and experiment. Qualitative comparisons between FE and experiments are shown inset at different normalized displacements. D. The effect of the fitting parameters  $a$ ,  $b$ , and  $\theta$  on the stress-stretch response.

transversely isotropic (cotton and nylon) material [6], [26]. Starting with the geometry of Jersey as a trigonometric curve [32], we modified the geometries of other patterns to match the topology while ensuring that the curve remains continuous and differentiable. A solid geometry is built from the centerline, and meshed using *quadratic tetrahedron elements (C3D10)*. The geometric parameters are determined from microscopic image of knit.

To render the simulations computationally feasible while realistically accounting for critical features such as yarn cross-sectional deformation, frictional contact, sliding, and stitch topologies, we define a representative unit to exploit a knit's periodicity (Fig. 3A). A minimum of four knots ( $2 \times 2$ ) is required to represent the different stitch patterns. To apply *periodic boundary conditions*, we identify periodic

geometry pairs (2 pairs in course and 4 in wale direction), and match the center nodes and planar orientations within (see the matching colored edges in Fig. 3A).

Macroscopic displacements are applied to both course and wale directions and the reaction forces are output during the load step. To address the difference in yarn diameter between its rest and knit state, a prior step is added to the model, where the yarn diameter is gradually increased using a temperature field to its final size [33], resulting in a variable cross-section depending on contact.

A custom biaxial stage applies equibiaxial stretch on the cruciform samples (Fig. 3B). An overhead camera (Raspberry Pi Camera Module 2) captures the deformation of the center square of the cruciform.

### Strain Energy Model

The mechanical responses of knit fabrics under biaxial stress are nonlinear and anisotropic (Fig. 3C). To facilitate analysis and isolate the effect of the knit parameters, we use the anisotropic part of a strain energy model based on the Holzapfel-Gasser-Ogden model [34], which is already implemented in commercial FE software including Abaqus:

$$\psi = \frac{a}{b} \left[ \exp \left( b (I_4 - 1)^2 \right) - 1 \right], \quad (1)$$

where  $a$  is an indicator of initial stiffness,  $b$  is a general indicator of stiffness, and  $\theta$  is an indicator of anisotropy (Fig. 3D). As  $\theta$  approaches  $45^\circ$ , the more the behavior in the course and wale directions become similar.  $I_4$  is the fourth stretch invariant, defined as:

$$I_4 = \left[ \mathbf{F}^T \cdot \mathbf{F} \right] : \mathbf{N} = \lambda_1^2 \cos^2 \theta + \lambda_2^2 \sin^2 \theta, \quad (2)$$

where  $\mathbf{F}$  is the deformation tensor,  $\mathbf{N} = [\cos\theta, \sin\theta, 0]^T$  is the direction of anisotropy, and  $\lambda_1, \lambda_2$  are the stretches in the course and wale directions, respectively. In this model, we assume plane stress with zero stress out-of-plane, so that the effect of anisotropy is planar. The corresponding first Piola-Kirchhoff stress (nominal stress) is therefore:

$$\begin{aligned} \mathbf{P} &= \frac{\partial \psi}{\partial \mathbf{F}} = \frac{\partial \psi}{\partial I_4} \frac{\partial I_4}{\partial \mathbf{F}} \\ &= 2a(I_4 - 1) \exp \left( b (I_4 - 1)^2 \right) [2\lambda_1 \cos^2 \alpha, 2\lambda_2 \sin^2 \alpha]^T. \end{aligned} \quad (3)$$

In the low-stress regime with  $I_4 \approx 1$ , this strain energy can be approximated by  $\psi = a (I_4 - 1)^2$ . As illustrated in Eqs. 1 and 3, both the strain energy and stress expressions include terms from the course and wale directions ( $\lambda_1, \lambda_2$ ). This indicates that deformations in the course and wale directions are coupled.

We compare the behavior of fabrics depending on stitch length, pattern, and material using  $a, b$ , and  $\theta$ . The parameters are fitted to the stress-strain curves obtained experimentally and through simulations. We use the Mesh Adaptive Direct Search (MADS) algorithm to find the optimal parameters by

minimizing the squared-difference of the simplified model and the stress-strain response [35]:

$$\operatorname{argmin}_{\mathbf{x}} \sum_{i \leq n} \| \mathbf{S}_i - \mathbf{P}_i(\mathbf{x}) \|^2 \quad (4)$$

where  $n$  is the sample size,  $\mathbf{x} = [a, b, \theta]^t$ ,  $\mathbf{S}_i$  represents the measured nominal stress for the  $i$ th sample, and  $\mathbf{P}_i$  denotes the resulting nominal stress from the strain model with the given parameter  $\mathbf{x}$ .

### Results from the Systematic Testing of Knitting Variables

We argue that the mechanical behavior of the knit fabric becomes most representative after preliminary loading, once the fabric has stabilized and further testing yields no significant changes. In this stabilized state, we perform two equibiaxial experiments on  $n = 3$  fabric samples for each variation in stitch length, pattern, and material. The results are shown as stress-strain curves of the experimental, simulated, and fit data in Fig. 4. The responses are fit using the strain energy model and shown in Fig. 5. All results are shown for the course direction only; results for the wale direction are in SI Section 6.

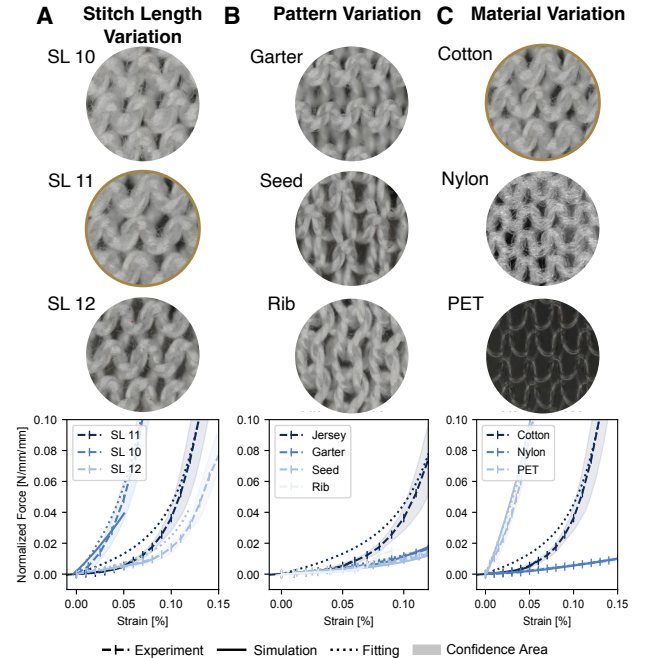


Fig. 4: Varying microstructure and mechanical response of three types of knit variation in the course direction: A. stitch length, B. pattern, and C. yarn material; the benchmark SL11, Jersey, Cotton is represented twice with a yellow outline; the normalized force-displacement curves show the experimental, simulated, and fit responses for three values in each category; the shaded area represents  $\pm$  one standard deviation from the mean.

Figure 5A highlights that stitch length primarily influences overall stiffness ( $b$ ), with shorter stitch lengths increasing stiffness. Altering the pattern has the greatest impact on fabric anisotropy, as changes in pattern directly affect the

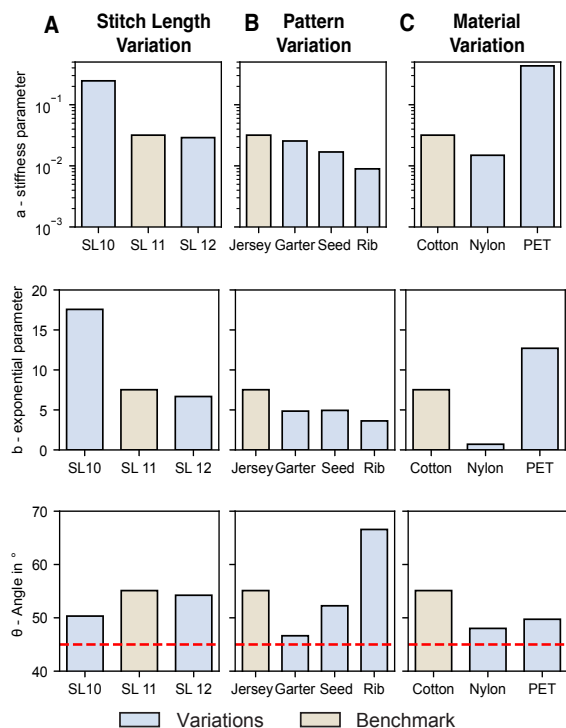


Fig. 5: For three types of variations, the plots show the fitting parameters  $a$ ,  $b$  and  $\theta$  of the strain energy model, where the red line at  $\theta = 45^\circ$  indicates identical stress in course and wale directions under equibiaxial loading.

symmetry of the fabric (Figure 5B). Material variations affect both initial stiffness ( $a$ ) and overall stiffness ( $b$ ) by an order of magnitude, but not anisotropy (Figure 5C).

These results make clear that each variable — stitch length, pattern, and material — affects different aspects of the mechanical response. Collectively, they offer practical design guidelines for tailoring the behavior of homogeneous fabrics. Specifically, material selection defines the overall stiffness range, pattern choice determines the degree of anisotropy, and stitch length serves as a fine-tuning parameter to achieve the desired stiffness response.

### Numerical validation

The numerical results and the proposed strain energy model were validated against experimental data by calculating the normalized root mean squared error (NRMSE), normalized by the maximum stress value, for each variation. The normalized error was below 5%, with two exceptions for all simulations and strain energy models. At a stitch length of 10, the simulation error reached 12.3%, attributed to the tightly knotted configuration leading to increased contact interference within the knit structure. At a stitch length of 12, the model’s fit error was 10.7%, reflecting the model’s compromise in fitting the strain energy across both the course and wale directions. This balancing act can introduce discrepancies, as the model aims to capture behavior across multiple deformation modes.

Industrial knitting machines can vary the above parameters within the same piece of fabric. In fact, heterogeneous fabrics are necessary to achieve spatially varying functionalities. We begin by studying the effect of spatially transitioning from one parameter to another within the same fabric.

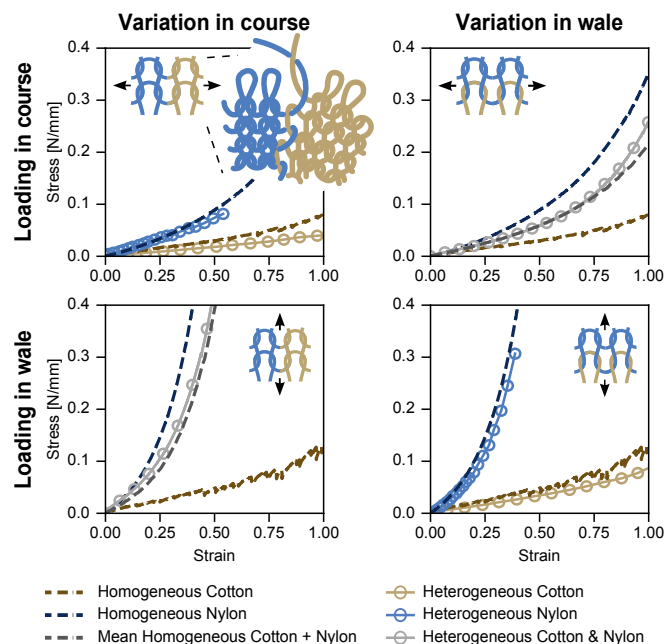


Fig. 6: Results for uniaxial testing of homogeneous vs. heterogeneous swatches of cotton and nylon; material variation occurs along the course (right column) and wale (left column) direction; testing occurs *in parallel* (top row) and *in series* (bottom row).

Heterogeneous variations can occur both in course and wale directions (see diagrams in Fig. 6). Change in material in the course direction requires a transition technique called intarsia, where new variation is knit into a new column (see drawing in Fig. 6). In the wale direction, the change occurs seamlessly, since a row of knots of a length, pattern, or material can be directly knit into a different row.

Here, we present results for material changes, which had the largest impact on mechanical behavior of homogeneous specimens. The results for variations in patterns are given in SI Section 6. As we aim to isolate the effect of the transition from one mechanical regime to another, we impose uniaxial stress on the samples. We subject an initially square knit fabric ( $l, w = 50\text{mm}$ ) using two different yarn materials (nylon and cotton), varied in the course and wale directions, up to 100% strain in both course and wale directions (total of four tests). When the sample is tested such that both materials are clamped together on both sides (material change is in line with the testing axis), we say the sample is tested *in parallel*. Conversely, when the material change is perpendicular to the testing axis, we say the sample is tested *in series*. For the *in parallel* test scenario, both fabrics are subjected to the same amount of strain. For the *in series* test scenario, we

use digital image correlation (DIC) to track the displacement of the transition line between materials to extract the strain experienced by the two parts of the fabric.

We compare the resulting behavior against those of homogeneous fabrics under the same testing condition to extract the influence (if any) of the transitions. When testing *in parallel* (Fig. 6 top row), we see that the heterogeneous response is closely approximated by the average response of homogeneous swatches. When testing *in series* (Fig. 6 bottom row), we see that the individual material response is in line with the individual testing of homogeneous swatches, showing that material transition does not influence the behavior of the fabric.

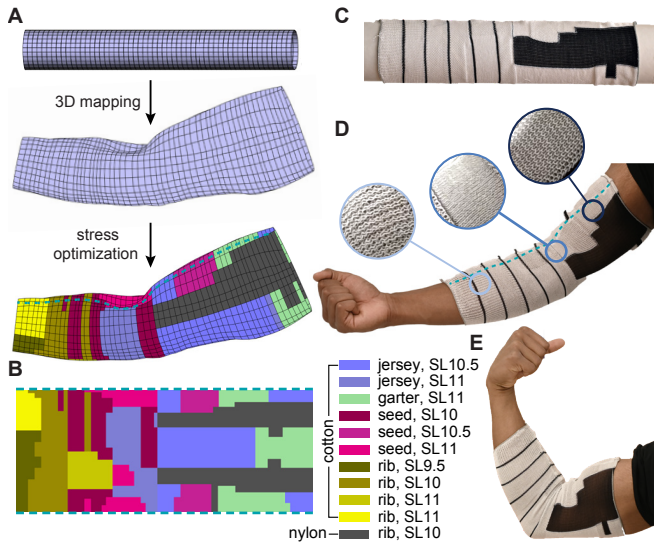


Fig. 7: Design of a tubular sleeve that results in constant stress magnitude when worn. A. A tubular geometry when knit with the wrist diameter as a reference is mapped to accommodate a muscular arm, after which knit variables are optimized to achieve uniform stress distribution; B. The resulting knit pattern with different regions assigned different stitch length, material and pattern; C. correspondence between the digital design and the physical specimen when stretched uniformly on a cylinder; D. The sleeve exhibiting variable stretch when worn on the arm, and the knit microstructure that enable this; E. the sleeve further accommodates muscle flexing when bend; the teal threaded line in A, B, and C indicates the seam position.

#### DESIGN OF A UNIFORM STRESS SLEEVE

For skin-tight garments such as bodysuits, compression sleeves, and leggings, some stretch is present throughout the fabric to reduce wrinkling. To account for the varying stretch across different parts of the human body, *e.g.*, different circumferences between the bicep and the wrist, additional panels are often sewn in. These extra panels reduce fabric damage from excess stretch and alleviate discomfort associated with large compressive stress to the body. (As shown earlier, generally, stress increases exponentially with stretch.) However, achieving uniform compression with paneling is

challenging and produces fabric waste. The additional seams can also cause skin irritation and introduce weaknesses in the garments [36]. Building on the results above, we demonstrate a single piece of simply shaped heterogeneous fabric that can accommodate spatially varying stretches while maintaining the uniform stress distribution throughout. In contrast to previous work that uses thermal actuation for self-fitting after production [10], [37], [38], our approach is to optimize the topology *a priori* for fit and uniform stress distribution.

Using the arm as an example, we reconstruct the arm of a muscular volunteer in three dimensions. By generating a quadrilateral mesh and mapping it onto a regular cylinder with a radius matching that of the wrist, we derive the strain experienced at each material point on the arm (Fig. 7A). We then identify knit parameter combinations that produce consistent stress under these varying strains (Fig. 7B). This results in a uniform stress as possible, even though different parts of the sleeve may experience dissimilar strains when it is worn. We verify that the fabric stretches as predicted by the design on the scanned arm, with no slack observed (Fig. 7D).

This work establishes a robust and accurate experimental and numerical framework for predicting and tuning the mechanical behavior of industrial knit fabrics, enabling precise control over stiffness, anisotropy, and spatially varying functionalities. By integrating computational modeling, simplified energy-based homogenization, and scalable manufacturing, our approach enables the streamlined design and production of optimized, personalized textiles—opening new frontiers in wearable devices, functional fashion, and beyond.

#### MATERIALS AND METHODS

##### Manufacturing of knit specimens

We use a Stoll CMS 330 industrial knitting machine to knit the fabric swatches. The patterns are manually programmed except for the sleeve, which is generated algorithmically. Detailed information is given in SI Section 1.

##### Yarn experimental testing

The yarns are washed and dried prior to mechanical loading. In tension, the yarns are loaded from the relaxed state (50 mm) until failure at a rate of 0.1 mm/s. The diameter of the yarns are measured throughout. In compression, the yarns are pre-tensioned until their diameter match those of the yarns in knit fabrics. They are then compressed at a rate of 0.01 mm/s up to a threshold of 50 N. A universal testing machine (Instron 68SC) is used in all tests. Additional details on the procedure are given in SI Section 2.

##### Fabric swatch experimental testing

The homogeneous specimens are laser cut to a cruciform shape such the loads are applied to a  $30 \times 30$  mm gauge area, except for the PET samples which are cut to a square shape due to unravelling at the corners of the cruciform.

All specimens are washed and dried prior to mechanical testing. Optical microscopy is used to obtain the geometrical parameters for FEM. All homogeneous specimens are tested

## I. FABRICATION PROTOCOL

## A. Fabrication instructions

All specimens featured in this manuscript are knit using CMS 330 (STOLL). The CMS 330 is a versatile flatbed knitting machine, designed for both technical textiles and fashion applications. With a working width of 36 inches and support for 12 and 14 gauge needles, it is equipped with three fully functional knitting and transfer systems, a weave-in device. This machine allows for complex structural changes and manipulations. Front to back stitch transfers with a series of racking actions allow for change of structure and pattern type. Individual needle placement changes length of stitch, which adds to the complexity of structural possibilities.

STOLL knitting machines use their own coding language, *Sintral*. This can be controlled through a STOLL provided software (*MIPlus* or *CreatePlus*). Default knitting files have standard settings for stitch length, speed, take down and racking placement. Each knit file is designed using the *MIPlus* software and then processed out into *Sintral* language.

At the knitting machine, these files are directly uploaded with a user interface display which can allow for potential, but more limited change within the aforementioned settings. Yarns must be manually installed, and thread through a series of tension apparatuses. These tensioners must be then manipulated by hand depending on yarn properties.

## B. Fabrication parameters

Homogeneous fabric swatches are all knit with repeated dimensions of 100 stitch wide and 100 row long. Change of stitch length, pattern type and yarn are substituted in between swatches. Small changes in programming, while may seem subtle can often cause great and unexpected varying difference between swatches. As a result, a qualifier in our set of tested knit swatches was the ability to leave all setting at their default when not being tested. The largest factor in this parameter was the fabric takedown. The takedown is how quickly the fabric is being pulled downward while knitting. It first begins through the comb apparatus and then eventually a set of rollers. With very large stitch length or varying stitch length across the knitting bed, if the takedown is too slow, the stitches begin to plume upward. This can cause dropped stitches. Where if the takedown is too high, it can begin to break the yarn. While the stitch length can be the same in two swatches, a change in takedown will vary the results. As a result, the takedown never changed from default settings but created certain barriers at the extreme ends of stitch length variation or pattern types with more involved transfers.

## II. YARN EXPERIMENTS

We quantify the tensile and compressive behavior of yarns used to knit the fabrics. Since the numerical models assume the yarns to be homogeneous solids, we experimentally obtain the homogenized properties of the yarns as input [40]. When a fabric swatch is deformed, the yarns experience tension along their length and compression in the orthogonal

using a custom biaxial testing stage (Fig. 3B). The specimens are clamped on all four edges. Equibiaxial strain is applied up to 30%. The actual strain in the gauge area is captured with an overhead camera. Three specimens are loaded cyclically three times each for each parameter variation.

Uniaxial testing is conducted to measure the influence of the different transitions (heterogeneous samples) using specimens of  $50 \times 50$  mm. Further details on the testing procedures can be found in SI Sections 3 and 4. Both are based on previous testing procedures described by Connolly et al. [39].

*Numerical modeling of knits*

ABAQUS/Standard 2022 is used to simulate the mechanical behavior of knit fabrics. The rest configuration of the knit geometry is described by a space curve parameterized along its arc length. A  $2 \times 2$  representative unit is defined and meshed using quadratic tetrahedral elements. Two static loading steps with nonlinear geometry are defined: The first uses thermal expansion to prevent any interference while allowing proper contact between the yarns. The second applies prescribed displacements in the two directions. This procedure is detailed in SI Section 7.

*Design of the sleeve*

A 3D scanned arm is used as the target shape. A cylinder with a circumference equal to that of the wrist is used as the initial geometry. The resulting strain on each mesh is estimated by generating a structured quadrilateral mesh on both the initial and target geometries with the same number of elements and a one-to-one mapping. The yarn material is initialized as cotton for all meshes. Due to peak stresses exceeding the yield stress of our cotton yarn, we switched certain regions to Rib nylon, which is more compliant. The homogenized model is used to predict the resulting stress based on the knit parameters—stitch length, pattern, and material—at these estimated strains. The parameters minimize variance in stress distribution throughout the fabric. The optimized parameters are filtered to obtain contiguous parameter regions. The details in selecting excessive strain region, filtering and optimization are state in SI Section 9, fabrication and experiments. The final design is processed using CREATE PLUS (Stoll) and knitted using the Stoll CMS 330.

## ACKNOWLEDGMENTS

We thank Lavender Tessmer for her guidance and early collaboration in industrial knitting. We thank Ushanth Balasuriya for volunteering his arm. Some of the computing for this project was performed on the Stanford University Sherlock cluster. We would like to thank Stanford University and the Stanford Research Computing Center for providing computational resources and support that contributed to these research results. We also thank Conor O'Brien at Otherlab for his advice and support in knitting the sleeve.

direction due to yarn-yarn interactions. This simplification enables us to assume transversely isotropy for multi-filament yarns, and isotropy model for monofilaments.

As outlined in the main text, we use three types of yarn: cotton (Supreme Corporation), nylon (Hickory Throwing), and PET (The Thread Exchange). Prior to testing, the yarns are washed in 30 °C water and dried in 70 °C convection chamber. Microscopy reveals that the geometry of the yarns differs qualitatively in their rest state (Fig. 1, main text). Cotton consists of two plies of natural discontinuous fibers wound together, nylon exhibits bunching of highly curved, intertwined continuous fibers, and PET is a monofilament that remains locally straight.

Additionally, it is observed that the diameter of the yarns within the knit structure may differ significantly from that of free-standing yarns, suggesting that some yarns are naturally pre-tensioned when incorporated into the fabric (Table I). This effect is most prominent for nylon.

TABLE I: Diameter of the yarns pre and post washing, and in a knit swatch

	Pre wash [mm]	Post wash [mm]	In knit [mm]
Nylon	1.644	0.951	0.334
Cotton	0.416	0.445	0.444
PET	0.177	0.177	0.178

To estimate the pre-tension of the yarns within the fabric and the corresponding diameter, we conduct simple experiments by progressively adding mass to a yarn of 180mm in initial length and measuring the change in diameter under a microscope and the change in yarn length (Table II, Fig. 8).

TABLE II: Measurements of the nylon yarn length and diameter under force-controlled loading

Length [mm]	Displacement [mm]	Diameter avg. [mm]	Force [N]
180.0	0	0.951	0
206.0	26.00	0.874	0.001460
225.5	45.50	0.763	0.002920
246.0	66.00	0.616	0.004390
262.0	82.00	0.562	0.005850
273.0	93.00	0.475	0.007310
280.0	100.0	0.432	0.00877
292.4	112.4	0.393	0.01023
295.0	115.0	0.390	0.01169
297.4	117.4	0.362	0.01316
299.0	119.0	0.350	0.01462

To validate this and obtain the entire force displacement curve, we apply tension to the yarns until failure using a universal testing machine (Instron 68SC-2). Yarns are dimensioned to a 50 mm gauge length in the rest state. Displacement is applied at 0.1 mm s<sup>-1</sup>. By applying tension using the tensile testing machine, we expect the first portion of the force displacement curve to reflect the above manual test with nylon for forces between 0 N and  $F_{pt}$ . At  $F_{pt} \approx 0.0146$  N, the yarn is at the diameter  $d_k \approx 0.350$  mm in the knit (Fig. 8C). The small deviation results from the limitation

of the manual testing method and the difficulty to measure the initial length of a free-standing nylon yarn (Fig. 8D).

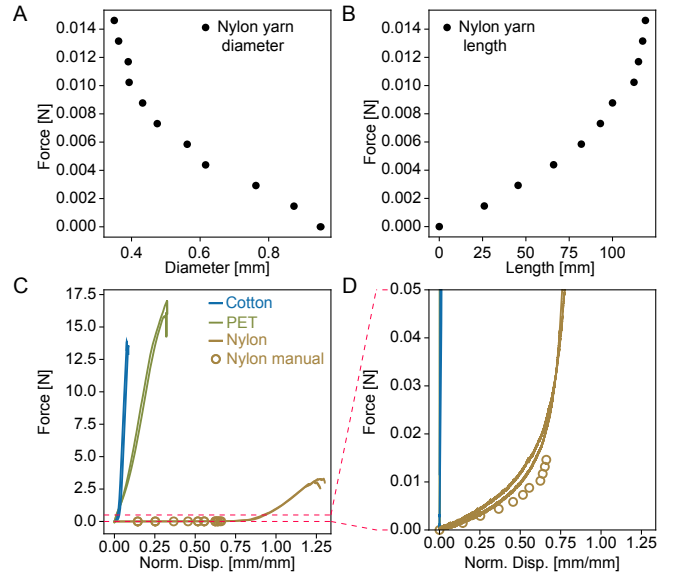


Fig. 8: Diameter (A) and Length (B) measured for increasing load for nylon yarn. Force-Displacement curves for uniaxial tensile testing of the three yarns; dashed line is  $F_{pt}$ ; overall behavior shown in (C) and adjusted scale for small forces shown in (D).

We then obtain the compressive force displacement behavior of the yarns in the lateral direction. Due to the extremely small force and displacement, we overlay ten yarns in parallel to magnify the reaction forces (Fig. 9a).

Each yarn is pre-tensioned to  $F_{pt}$  prior to being affixed to the bottom fixture. Therefore, the initial diameter matches the ones discussed above  $d_k$ . We then apply compression through the top plate (gauge width 25 mm) at a rate of 0.01 mm s<sup>-1</sup> up to a threshold of 50 N. For cotton and PET,  $F_{pt}$  is negligible since the diameter does not change significantly between a free yarn and in a knit. The results are shown in Figure 9.

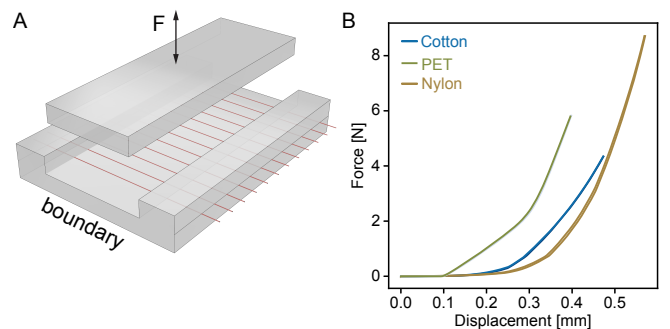


Fig. 9: (A) Test setup for compression; (B) Force-Displacement curves for compression tests.



### III. BIAXIAL EXPERIMENTS

#### A. Bistable stage

Biaxial testing is performed to understand the material behavior under multi-directional stresses, which is essential for knit fabrics that face complex loading in real-world scenarios. To enable biaxial testing of flexible materials over large strains, we custom built a biaxial stage using commercial load transducers, linear stages and microcontrollers (Fig. 10).

Four motorized linear stages are positioned orthogonally on a breadboard (Thorlabs). Each stage has a maximum displacement of 300 mm. Force measurement is facilitated by the load transducers affixed to two orthogonal linear stages. It records data at approximately 5 Hz. An overhead Pi Camera 3 is installed above the specimen. All components (4 linear stages, 2 load transducers and the overhead camera) are connected to a Raspberry Pi 4 micro-controller. Through the microcontroller, users can setting of parameters including preload, strain, strain rate, and specimen size.

#### Specimen preparation

Each fabric swatch undergoes a series of preparatory steps prior to testing. First, the initial as-knit dimensions are measured. The fabrics are then soaked in 30 °C water for 15 minutes, dried at 70 °C. We then measure the post-wash dimensions to calculate shrinkage. Microscopy is used to obtain the microstructural geometry of the knit fabrics.

To prepare the biaxial test samples, we used a CO<sub>2</sub> laser cutter (Trotec Speedy 360) to cut cruciform specimens from the fabric swatches (Fig. 11 left). Each specimen has a 30 × 30 mm gauge area, and 20 mm extension in each direction to be clamped and attached to the grips (Fig. 11 right). Note that clamps are affixed to the fabrics using bolts. They are then slotted onto the grips on the biaxial machine. This minimizes the bending force imposed on the sensitive load transducers.

#### B. Biaxial testing

A displacement rate of 0.5 mm s<sup>-1</sup> is set to a maximum strain of 0.3 of the gauge length. Each sample undergoes three cycles of tensile loading and unloading, and three specimens were tested per specimen type. DIC is used to track the deformation of the gauge area of the fabric to obtain the true strains.

### IV. UNIAXIAL EXPERIMENTS

Heterogeneous fabrics are composed of regions with different knitting parameters. Here we vary knitting pattern and yarn material to assess the effect of the transition that the knitting machine automatically imposes. For each combination, four tests are conducted (Fig. 12), reflecting the two loading directions (coarse and wale) and two transition directions (from loop to loop and from row to row).

Samples are cut with a gauge area of 50 mm (length) by 50 mm (width). Uniaxial stretch is applied using an Instron static load testing machine at a displacement rate of 0.5 mm s<sup>-1</sup> and a maximum strain to 100 %. Three cycles

are conducted. For specimens tested in series, the position of the transition line is tracked using DIC. For each parameter combinations, a homogeneous fabric is also tested to serve a benchmark of comparison.

### V. PRELIMINARY FABRIC TESTING RESULTS

Knits are complex physical systems whose mechanical response may have many contributing factors. Prior to systemically parametric sweep, we examine the relative significance of four factors: 1) cycling testing of increasing maximum strain, 2) effect of washing and drying, 3) yarn sliding and friction, and 4) local damage.

#### A. Cyclic testing of increasing maximum strain

First, we examine the effect of biaxial cyclic loading by subjecting the same fabric specimen (Jersey, cotton, SL11) to increasingly larger strain from 0.05 to 0.35 in both directions. The results are shown in Fig. 13. First, we note there is significant hysteresis between the loading and unloading force-displacement curves. Second, the fabrics exhibit softening, *i.e.*, the behavior is stiffer during initial loading up to a terminal strain as compared to subsequent loading to that same strain. Similar phenomenologically to the Mullins effect, the force displacement behavior depends on the maximum strain previously encountered. The underlying physics could be explained by the sliding and internal dislocation of yarns within a knit during during the initial loading, resulting in a permanent increase in the rest lengths.

#### B. Effect of washing and drying

Washing and drying is a common protocol listed in standardized testing of fabrics prior to mechanical characterization [41]. By washing and drying the fabrics, we may significantly change their internal microstructure by relaxing the pre-tension imposed during the knitting process. Since most fabrics will undergo many washing and drying cycles over their lifespan, the mechanical response of fabrics after washing is more representative of their behavior during operation.

To quantify the effect of washing, we first observe the geometry of a swatch before and after the process. Different yarn materials exhibit different levels of shrinkage. This is explained by examining the microstructure of the yarn. The nature of synthetic fiber such as nylon consists of continuous fibers that are bent and twisted. The tension applied during knitting causes the fibers to straighten, and enlarge the overall size of the fabric swatch. After washing, the swatches shrink nearly isotropically by 25%.

To ensure the repeatability of our results and to record force/displacement data relevant to a fabric's lifespan, we conduct 15 equi-biaxial tests, washing and drying the fabric before the 1st, 6th, and 11th cycle. As shown in Fig. 14, the first tests after each washing remain different from subsequent tests. The initial response partially recovers following a wash. The size of the specimens also recovers to 50 × 50 mm. This suggests that upon washing, the yarns are able to partially recover their original morphology. This is different from Mullin's effect where the softening is irreversible.

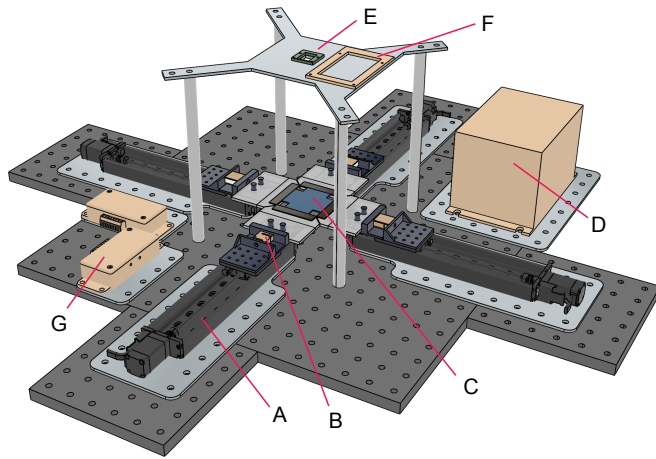


Fig. 10: Biaxial stage construction and elements.

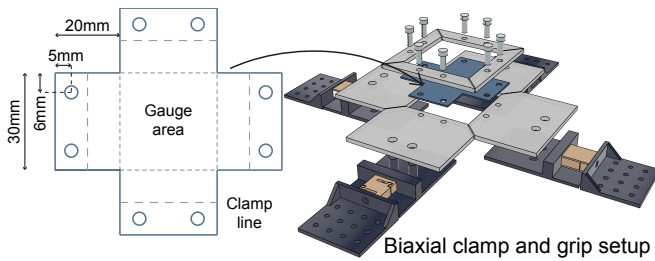


Fig. 11: Fabric swatch geometry (left) and test setup (right).

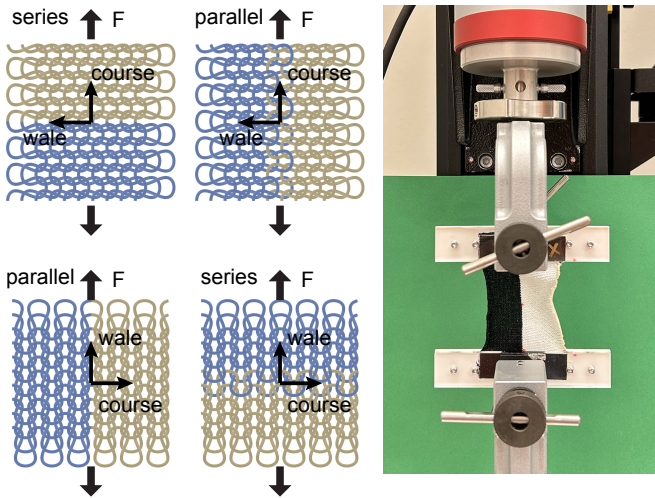


Fig. 12: Four different testing conditions for heterogeneous fabrics made using two sets of parameters.

### C. Effect of friction

We aim to understand the mechanisms through which strain energy is dissipated during loading and unloading. Using the most irregular yarn (nylon) and double-ply yarn (cotton), we test two specimens (after washing, previously untested), lubricating one using silicone oil. The resulting normalized force-displacement show that, for nylon, the initial stiffness decreases with lubrication. This is only notice-

TABLE III: biaxial stage component list

NO.	Model	Description
A	Zaber LSM50A-E03T4A	Motorized linear Stage
B	RES2-5KG	Load transducer
C	Specimen	Cruciform fabric specimen
D	Zaber X-MCC4	Linear stage controller
E	Pi Camera 3	Camera
F	Raspberry Pi 5	Micro controller
G	Loadstar AI-1000	Amplifier for Load Transducer

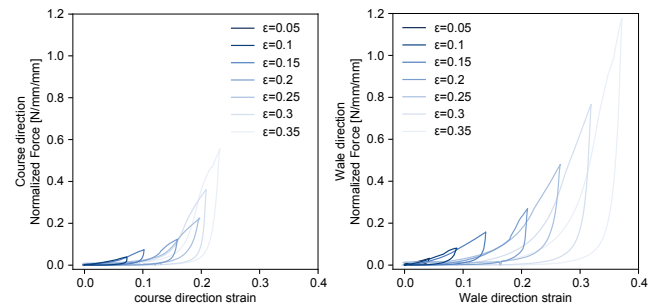


Fig. 13: Force displacement behavior the same fabric specimen (Jersey, cotton, SL11) undergoing cyclic strain of increasing magnitude to exhibit softening effect.

able for the initial loading. The response of the subsequent tests are not affected by lubrication (Fig. 15). The behavior for cotton does not change noticeably.

### D. Viscoelastic effect

Another contributor to energy dissipation in a knit fabric may be viscoelasticity. We examine this using knits from two yarn materials (nylon and PET) and impose strain-rates of  $\dot{\epsilon} = \{0.1, 0.5, 1, 5\}$ . To isolate this effect, we use specimens that have been previously cycled and reached a steady-state (cycle # larger than 5) to ensure repeatability. By increasing the strain rate, we do not observe a large change in the response in nylon. This suggests that the filaments within the nylon yarns themselves do not experience significant strain. Rather, it is the straightening of local curvature that accommodates the global strain. With PET, due to the nature of the monofilament, a small but consistent increase in stiffness is observed. This is most evident at larger strains where, we hypothesize, the fibers themselves are elongated.

Once knit stitches are plastically deformed, they predominantly undergo rigid body movement during unloading and subsequent loading events.

a) *Local damage*: At larger strains, there are localized drops in the force response. This is best illustrated by observing PET monofilament knits. We subject a specimen

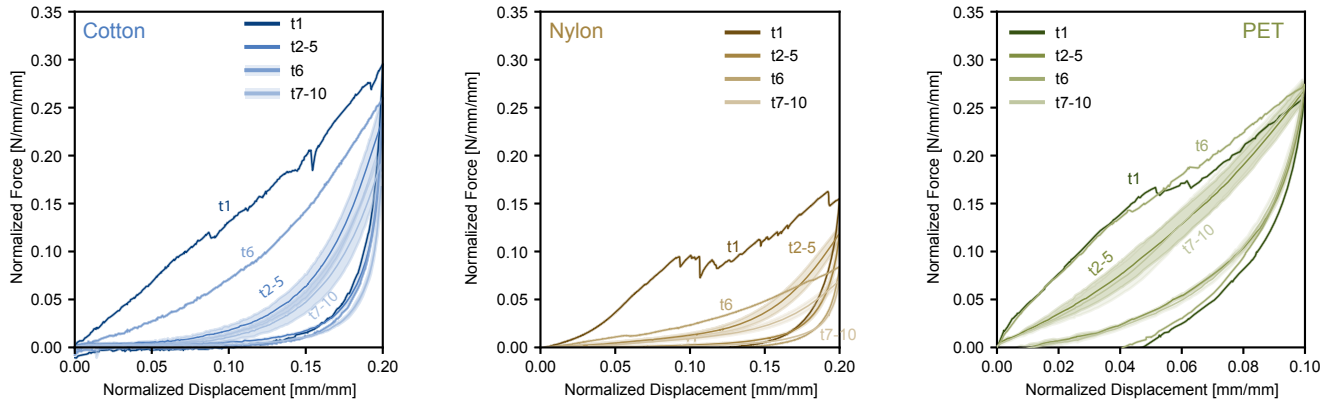


Fig. 14: Force displacement behavior of fabric swatches made from different yarn materials after repeated washing and testing.

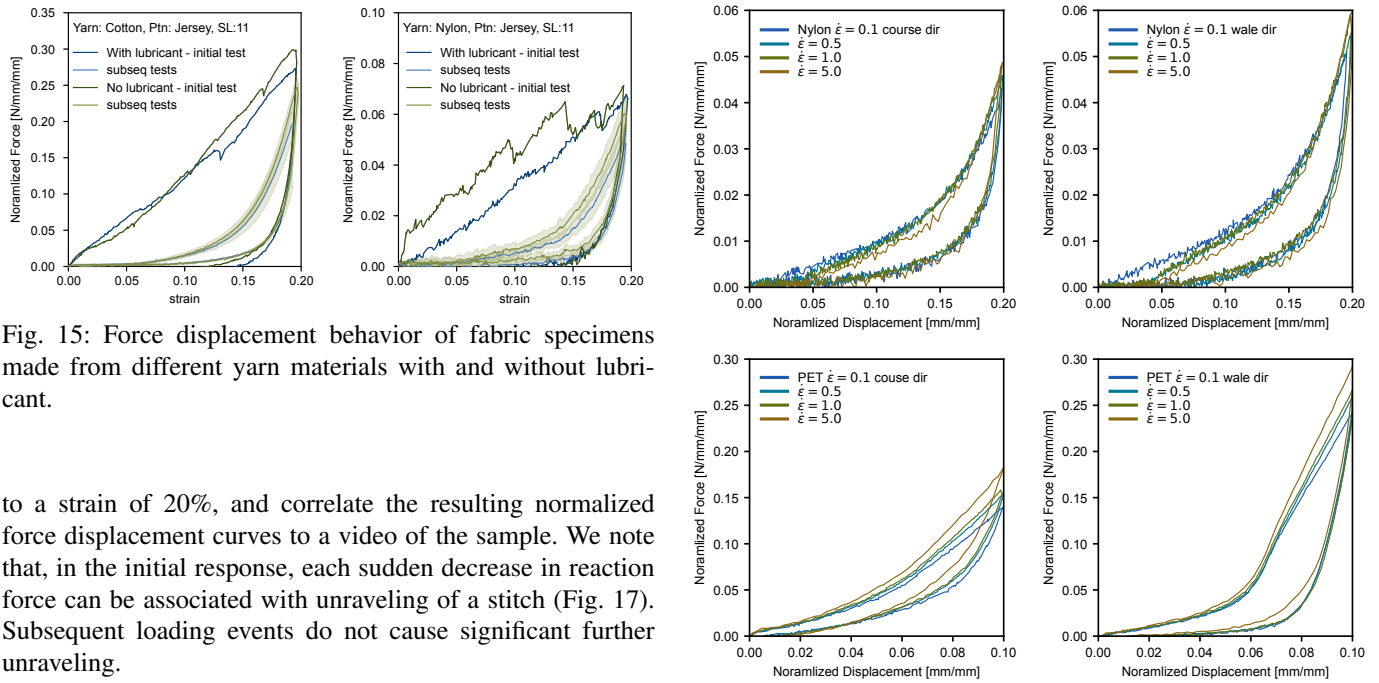


Fig. 15: Force displacement behavior of fabric specimens made from different yarn materials with and without lubricant.

to a strain of 20%, and correlate the resulting normalized force displacement curves to a video of the sample. We note that, in the initial response, each sudden decrease in reaction force can be associated with unraveling of a stitch (Fig. 17). Subsequent loading events do not cause significant further unraveling.

## VI. ADDITIONAL EXPERIMENTAL RESULTS

### A. Homogeneous knit fabrics

In this section, we report the results for the knit variations in the wale direction in Fig. 18, since only those in the course direction are shown in the main text for brevity. We also add Tables IV and V listing all the normalized root mean squared errors (NRMSE) in the course and wale directions normalized by the maximum stress value that are referred to in the main text.

### B. Heterogeneous knit fabrics

In this section, we report the results for heterogeneous fabrics where the pattern is varied both in the wale and the course direction in Fig. 19, since only the heterogeneous results for varying materials were reported in the main text.

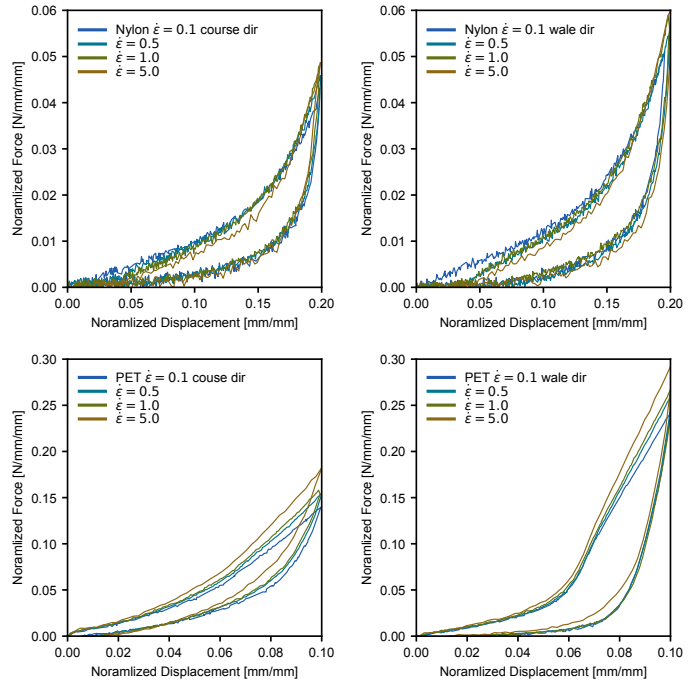


Fig. 16: Nylon (top row) and PET (bottom row) response at different strain rates to test viscoelasticity in the course direction (left column) and the wale direction (right column).

## VII. NUMERICAL MODELING

### A. Model Definition

1) *Geometry*: We consider four fundamental patterns: jersey, garter, rib, and seed. The centerline geometry of these patterns are constructed using sinusoidal space curves, building on previous work on the jersey pattern [42]. The period of the trigonometric functions is modified to reflect the symmetry of each pattern. The geometric parameters are measured from the actual fabric using microscopy. The space

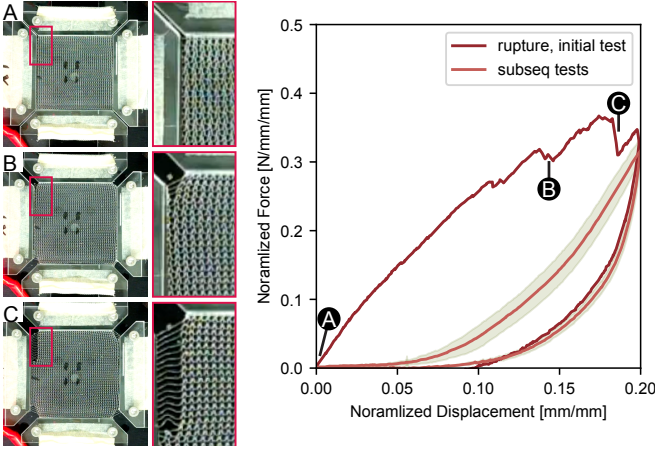


Fig. 17: Correspondence between sudden drops in force response and unraveling of yarns at the boundary.

TABLE IV: Normalized root mean squared error between the experimental data and the simulation (Sim) and the strain energy model (Fit) in the course direction (NRMSE), normalized by the maximum stress value for each variation (stitch length, pattern, material); the benchmark is SL 11, Jersey, Cotton.

Benchmark		SL 10		SL 12	
Sim	Fit	Sim	Fit	Sim	Fit
0.0480	0.0664	0.0943	0.0837	0.0333	0.107
Garter		Seed		Rib	
Sim	Fit	Sim	Fit	Sim	Fit
0.0408	0.0108	0.0191	0.0143	0.0498	0.0313
Nylon		PET			
Sim	Fit	Sim	Fit		
0.0217	0.0110	0.0945	0.0104		

curves for the four patterns are presented below.

$$\begin{aligned}
 \gamma_{st,k}(t) &= \left[ \frac{W}{2\pi}(t + a \sin 2t), h \cos t + kw, d \cos 2t \right], & \forall t \in \mathbb{R} \\
 \gamma_{g,k}(t) &= \left[ \frac{W}{2\pi}(t + a \sin 2t), h \cos t + kw, (-1)^{k-1} d \cos t \right], & \forall t \in \mathbb{R} \\
 \gamma_{r,k}(t) &= \left[ \frac{W}{2\pi}(t + a \sin 2t), h \cos t + kw, \frac{(-1)^n}{2} d (\cos 2t - 1) \right], & \forall t \in [(2n-1)\pi, (2n+1)\pi], n \in \mathbb{Z} \\
 \gamma_{sd,k}(t) &= \left[ \frac{W}{2\pi}(t + a \sin 2t), h \cos t + kw, 0.336(-1)^{k+n-1} d (\cos 3t - \cos t) \sin 2t \right], & \forall t \in [(2n-1)\pi, (2n+1)\pi], n \in \mathbb{Z}
 \end{aligned} \tag{5}$$

where the first subscript indicates the type of pattern with  $st, g, r, sd$  corresponds to stockinette, garter, rib and seed respectively, and the second subscript  $k \in \mathbb{Z}$  means  $k^{\text{th}}$  row of the knit. This space curve is controlled by geometric parameters,  $a, W, h, d$  where  $a$  controls the curvature of the loop within a single stitch,  $W$  is the width of a single stitch,  $h$  and  $d$  are half-height and half-depth of the single stitch, and  $w$  is the spacing between rows. Note on the periodicity that stockinette has identical geometry for all stitches, where garter has alternating rows, rib has alternating columns and seed has alternating pattern for every rows and columns.

2) *Material Model*: An anisotropic linear elasticity model is applied to model the yarn as a transversely isotropic material in linear regime. When the material shows an isotropic behavior within a plane normal to the axis of symmetry, it is said to be a transversely isotropic material [43]. In linear elastic regime, there are 5 parameters that configure the material model:  $E_p, E_t, \nu_p, \nu_{pt}, G_t$ . The elasticity tensor

TABLE V: Normalized Root Mean Squared Error (NRMSE) between experimental data and simulation (Sim) as well as the strain energy model (Fit) in the wale direction. NRMSE is normalized by the maximum stress value for each variation in stitch length, pattern, and material. The benchmark configuration is SL 11, Jersey, Cotton.

Category	Variation	Sim	Fit
Stitch Length	Benchmark (SL 11, Jersey, Cotton)	0.0371	0.0279
	SL 10	0.1240	0.0982
	SL 12	0.0276	0.1270
Pattern	Garter	0.0284	0.0106
	Seed	0.0398	0.0184
	Rib	0.0457	0.0112
Material	Nylon	0.0112	0.0157
	PET	0.1130	0.0258

represented with these parameters is given below.

$$\begin{Bmatrix} \epsilon_{11} \\ \epsilon_{22} \\ \epsilon_{33} \\ \gamma_{12} \\ \gamma_{13} \\ \gamma_{23} \end{Bmatrix} = \begin{Bmatrix} \frac{1}{E_p} & -\frac{\nu_p}{E_p} & -\frac{\nu_{pt}}{E_t} & 0 & 0 & 0 \\ -\frac{\nu_p}{E_p} & \frac{1}{E_p} & -\frac{\nu_{pt}}{E_t} & 0 & 0 & 0 \\ -\frac{\nu_{pt}}{E_t} & -\frac{\nu_{pt}}{E_t} & \frac{1}{E_t} & 0 & 0 & 0 \\ 0 & 0 & 0 & \frac{2(1+\nu_p)}{E_p} & 0 & 0 \\ 0 & 0 & 0 & 0 & \frac{1}{G_t} & 0 \\ 0 & 0 & 0 & 0 & 0 & \frac{1}{G_t} \end{Bmatrix} \begin{Bmatrix} \sigma_{11} \\ \sigma_{22} \\ \sigma_{33} \\ \tau_{12} \\ \tau_{13} \\ \tau_{23} \end{Bmatrix}$$

$E_p, E_t$ , are Young's moduli in plane and longitudinal direction respectively. They are determined by the tensile and compression tests of the yarns.  $\nu_p$ , the Poissons' ratio within the plane is assumed to be 0.3.  $\nu_{pt}$ , the Poissons' ratio between the plane and longitudinal axis is estimated from the relationship between the longitudinal stretch and radius change.  $G_t$  is fitted to match the experimental data, and is not as significant as other parameters.

3) *Contact and preliminary step for geometry refinement*: There is a complex contact behavior between yarns from neighboring stitches. In our FE simulation, this contact behavior is modeled using the Abaqus/Standard contact module, incorporating tangential friction and hard normal contact. Any initial contact between yarns is treated as an interference fit. The tangential friction coefficient was determined through preliminary simulations to match experimental data: 0.2 for cotton, 0.8 for nylon, and 0.4 for PET monofilament.

In knitted fabrics, yarns often exhibit a nonuniform cross-section, particularly at intersections with neighboring stitches where complex bending and contact occur. If the geometry is generated by sweeping a circular cross-section along the centerline defined by Equation (5), overlapping interference between stitches may arise in these regions. Such interference can lead to mesh failures and numerical instability.

To address this issue, we implemented a preliminary load step in Abaqus. The simulation begins with a swept structure of reduced radius, which undergoes thermal expansion during this step to restore the original radius. The material is assigned a model-specific thermal expansion coefficient that is positive in the radial-tangential direction and zero or negative in the longitudinal direction. The initial radius, expansion

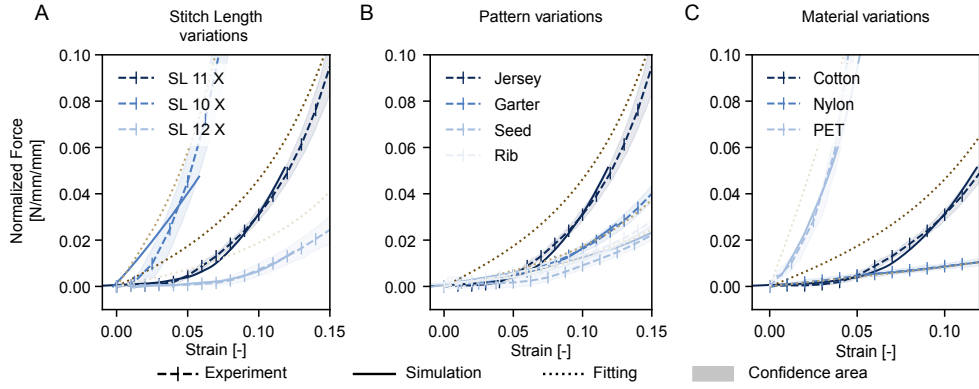


Fig. 18: Varying microstructure and mechanical response of three types of knit variation in the wale direction: A. stitch length, B. pattern, and C. material; the benchmark SL 11, Jersey, Cotton is represented twice with a yellow outline; the stress-strain curves show the experimental, simulated, and fit responses for three values in each category; the confidence area represents  $\pm$  one standard deviation from the mean.

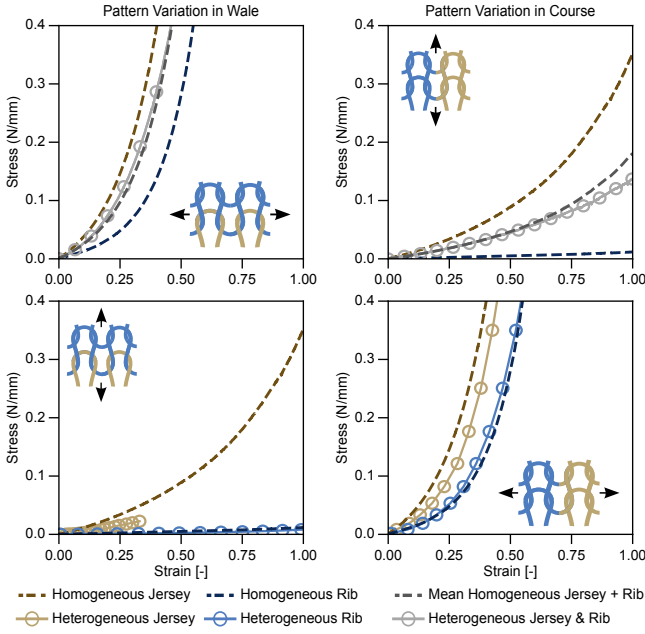


Fig. 19: Results for uniaxial testing of homogeneous vs. heterogeneous swatches of jersey and rib patterns; pattern variation occurs along the course (right column) and wale (left column) direction; testing occurs *in parallel* (top row) and *in series* (bottom row).

coefficient, and temperature increase were adjusted to produce a geometry that closely resembles the actual structure. This step enables contact-free regions to achieve the desired yarn radius while preserving the overall dimensions. The interaction between stitches forms a finite contact surface without interference or negative-volume meshes. Notably, this preliminary step improves contact modeling compared to circular beam elements, which can only represent contact as a line.

4) *Boundary conditions:* The periodic boundary conditions are applied so that the  $2 \times 2$  stitch lattice represents the

tessellated knit structure. The building block is defined by the centerline  $\gamma_{\cdot,k}(t)$  in (5), with  $k = 1, 2, 3$ , bounded by  $x \in (0, 2W)$ ,  $y \in (w, 3w)$ . There are six pairs of boundary nodes, for a total of twelve nodes.

- Horizontally aligned:

$$\begin{aligned} \mathbf{x}_{1,\text{left}} &= \gamma_{\cdot,1}(0) = (0, h + w, \cdot), \\ \mathbf{x}_{1,\text{right}} &= \gamma_{\cdot,1}(4\pi) = (2W, h + w, \cdot), \\ \mathbf{x}_{2,\text{left}} &= \gamma_{\cdot,2}(0) = (0, h + 2w, \cdot), \\ \mathbf{x}_{2,\text{right}} &= \gamma_{\cdot,2}(4\pi) = (2W, h + 2w, \cdot). \end{aligned}$$

- Vertically aligned:

$$\begin{aligned} \mathbf{x}_{3,\text{top}} &= \gamma_{\cdot,1}\left(\frac{1}{2}\pi\right) = \left(\frac{1}{4}W, w, \cdot\right), \\ \mathbf{x}_{3,\text{bottom}} &= \gamma_{\cdot,3}\left(\frac{1}{2}\pi\right) = \left(\frac{1}{4}W, 3w, \cdot\right), \\ \mathbf{x}_{4,\text{top}} &= \gamma_{\cdot,1}\left(\frac{3}{2}\pi\right) = \left(\frac{3}{4}W, w, \cdot\right), \\ \mathbf{x}_{4,\text{bottom}} &= \gamma_{\cdot,3}\left(\frac{3}{2}\pi\right) = \left(\frac{3}{4}W, 3w, \cdot\right), \\ \mathbf{x}_{5,\text{top}} &= \gamma_{\cdot,1}\left(\frac{5}{2}\pi\right) = \left(\frac{5}{4}W, w, \cdot\right), \\ \mathbf{x}_{5,\text{bottom}} &= \gamma_{\cdot,3}\left(\frac{5}{2}\pi\right) = \left(\frac{5}{4}W, 3w, \cdot\right), \\ \mathbf{x}_{6,\text{top}} &= \gamma_{\cdot,1}\left(\frac{7}{2}\pi\right) = \left(\frac{7}{4}W, w, \cdot\right), \\ \mathbf{x}_{6,\text{bottom}} &= \gamma_{\cdot,3}\left(\frac{7}{2}\pi\right) = \left(\frac{7}{4}W, 3w, \cdot\right). \end{aligned}$$

Two reference points are defined to control the relative displacement of boundary nodes:

$$\begin{aligned} \mathbf{x}_{\text{RP1}} &= (d_x, 0, 0), & \text{with } \mathbf{x}_{\cdot,\text{right}} - \mathbf{x}_{\cdot,\text{left}} &= \mathbf{x}_{\text{RP1}}, \\ \mathbf{x}_{\text{RP2}} &= (0, d_y, 0), & \text{with } \mathbf{x}_{\cdot,\text{top}} - \mathbf{x}_{\cdot,\text{bottom}} &= \mathbf{x}_{\text{RP2}}. \end{aligned}$$

Aligning with the biaxial tensile test, a displacement boundary condition was applied by constraining  $d_x$  and  $d_y$ .

Using the final displacement ratio in the course and wale directions from the experiment,  $d_x$  and  $d_y$  were increased linearly in that ratio. The simulation was stopped when the solver step time reached 0.00001% strain with numerical instability. It was conducted on Stanford Sherlock using normal compute nodes.

The cutting plane, which intersects the boundary nodes and is normal to the centerline at these nodes, will remain planar to ensure periodicity. One point on the centerline,  $\gamma_{,2}(2\pi)$ , is fixed to remove rigid body motion.

## VIII. DATA POST-PROCESSING AND FITTING

### A. Data truncation for pretension adjustment

It is important to maintain consistent mechanical conditions across different samples. However, variations in pretension were observed in the experimental data across samples, causing shifts in the stress-strain curves. This was due to initial slack when clamping the samples to the test setup. Therefore, the data corresponding to the initial region where stress remained constant due to slack was truncated. This ensured the stress-strain curves started from the same slope. Since the two axes in biaxial testing are coupled, their relationship was preserved by shifting the time domain rather than directly adjusting the strain domain. The starting point of the shift was treated as the undeformed state, and the undeformed dimensions were updated accordingly. To plot the experimental data, stress values were interpolated at evenly spaced points within the measured strain range for each dataset and then averaged. Note that this method does not preserve the coupled relationship between the two axes. Pretension was also considered in simulations by adjusting the undeformed geometry and slightly shifting the curve to align with the experimental data.

### B. Fitting to the strain energy model

We fit the biaxial testing results to the strain energy model described in Eq. (1) of the main text to compare the behavior of different fabrics. Since the material is anisotropic and the data were obtained from biaxial test that elongates in both directions, it is crucial to preserve the directionally coupled behavior. Additionally, shifts in stress-strain curves can alter the fitted parameters due to the nonlinearity of the strain energy model. Therefore, all data points from the shifted experimental data are used for fitting without averaging.

The NOMAD (Nonlinear Optimization by Mesh Adaptive Direct Search), one implementation of Mesh Adaptive Direct Search (MADS) algorithm, is employed for fitting. NOMAD is a derivative-free optimization method specifically designed to handle nonlinear and non-convex problems. It is useful for models where gradients are difficult to compute or do not exist. The optimization problem is formulated in Eq. (4) of the main text.

## IX. SLEEVE DESIGN, FABRICATION AND EXPERIMENTS

A 3D reconstructed arm is used as the target geometry, while a cylinder with a circumference equal to that of the wrist is created as the initial geometry. A structured

quadrilateral mesh is generated on both the initial and target geometries, with 25 elements in the radial direction and 56 along the arm, ensuring the same number of elements on both geometry. The anisotropic strain in each patch is estimated by comparing corresponding mesh pairs. As excessive radial strain is detected beyond the maximum strain that cotton knit fabrics can endure, large strain regions are selected and switched to nylon yarn with a rib pattern, which is the most compliant option. The nylon areas are assumed to experience larger strain due to low moduli of the nylon, while the strain values in the other regions are adjusted to maintain overall stretch. To ensure contiguous patches, strain values are clustered by implementing K-means clustering algorithm using both strain value and spatial information. The homogenized model based on the proposed strain energy model is then used to estimate the resulting stress under these strain, with the knit parameters of stitch length, pattern, and material. These estimates are used to identify optimal parameter combinations that minimize variance in stress distribution. The detailed pseudocode is appended at the end.

The final design is processed using CREATE PLUS and knitted using the *Stoll CMS 330*. Through a bitmap file generated by the above mentioned code, this artwork is transitioned into the CREATE PLUS software. Small variations are made in this stage to allow for better knitting results. This included areas of large varying stitch length and knit transfers along the same course. Like the homogeneous samples, there are no changes in the fabric takedown, which made areas of varying stitch length difficult to knit. (In other knitting instances, change of carriage speed and fabric takedown may have mitigated some of these problems)

Additional edits needed to be made to allow for the intarsia section to knit without problems and to maintain full integrity of desired design. Small additions of tuck stitches, and added rows for feasible yarn carrier directions accounted for this.

Areas of small striping are added into the file for purely visual effect. This occurred on the forearm section of the sleeve. These stripes did not disrupt structure and performance, rather they became visual markers for different pattern sections. The yarn used here is the same cotton as its surrounding.

The sleeve is knit as a flat sheet and then in post processing sewn together. This needed to be knit flat rather than in a round seamless tube, because the pattern types used follow a series of front to back bed transfers. The original homogeneous swatches are all knit full gauge, meaning knit on every needle. However, in order to knit in a seamless tube when transfers need to occur, you must knit half gauge, where every other needle is active. Knitting in half gauge would vary the results from the original samples tested. We believe the post processed sewn seam would be a less intrusive shift in results.

---

**Algorithm 1** Sleeve Design Optimization

---

- 1: Initialize meshes with edge lengths  $M_{ij}^{arm,k}$ ,  $M_{ij}^{tube,k}$  for  $k = \theta, z$  yarn type  $Y_{ij} = \text{Cotton}$ , patterns  $P_{ij} = \text{Jersey, SL11}$
  - 2: Define strain vector  $\epsilon_{ij} = (\epsilon_{ij}^\theta, \epsilon_{ij}^z)$  where
$$\epsilon_{ij}^k = \left( M_{ij}^{tube,k} - M_{ij}^{arm,k} \right) / M_{ij}^{arm,k} \text{ for } k = \theta, z$$
  - 3: **for**  $j$  such that row strain  $\sum_i \epsilon_{ij}^\theta > \epsilon_{max}^{\text{Cotton}}$  **do**
$$\Delta_{nylon} = \left( \frac{1}{n} \sum_i \epsilon_{ij}^x - \epsilon_{max}^{\text{Cotton}} \right) / \frac{1}{n} \epsilon_{max}^{\text{Nylon}} \quad \triangleright \text{Number of nylon meshes}$$
$$A = \{x | n(\{y | \epsilon_{xj}^k \leq \epsilon_{yj}^k\}) \leq \Delta_{nylon}\}$$
$$\epsilon_{aj}^x = \begin{cases} \epsilon_{max}^{nylon} & \text{if } a \in A \\ \epsilon_{aj}^x \frac{\sum_i \epsilon_{ij}^x - \epsilon_{max}^{nylon} \Delta_{nylon}}{\sum_i \epsilon_{ij}^x} & \text{if } a \notin A. \end{cases}$$
Set  $Y_{aj} = \text{Nylon}$  for  $a \in A$   $\triangleright$  Add nylon patches
  - 4: **end for**
  - 5: Group strain values and spatial information  $(\epsilon_{ij}, i, j)$  using K-means clustering algorithm
  - 6: **for** each cluster  $C_k$  and its centroid  $(e_k, \cdot, \cdot)$  **do**

Calculate nominal stress at strain  $e_k$  for every pattern and stitch length combination in the design space
  - 7: **end for**
  - 8: Identify optimal pattern and stitch length  $\Phi_k$  to minimize stress variance
  - 9: **for**  $k$  and  $(\cdot, i, j) \in C_k$  **do**
$$P_{ij} = \Phi_k$$
  - 10: **end for**
  - 11: Generate pixel images and files for knitting machine
-

## REFERENCES

- [1] D. Liu, S. Koric, and A. Kontsos, “A multiscale homogenization approach for architected knitted textiles,” *Journal of Applied Mechanics, Transactions ASME*, vol. 86, 2019.
- [2] W. P. Moestopo, A. J. Mateos, R. M. Fuller, J. R. Greer, and C. M. Portela, “Pushing and pulling on ropes: Hierarchical woven materials,” *Advanced Science*, vol. 7, p. 2001271, 2020.
- [3] Y. Wang, L. Li, D. Hofmann, J. E. Andrade, and C. Daraio, “Structured fabrics with tunable mechanical properties,” *Nature*, vol. 596, pp. 238–243, 2021.
- [4] J. U. Surjadi, B. F. Aymon, M. Carton, and C. M. Portela, “Double-network-inspired mechanical metamaterials,” *arXiv preprint arXiv:2409.01533*, 2024.
- [5] W. Zhou, S. Nadarajah, L. Li, A. G. Izard, H. Yan, A. K. Prachet, P. Patel, X. Xia, and C. Daraio, “Polycatenated architected materials,” *arXiv preprint arXiv:2406.00316*, 2024.
- [6] K. Singal, M. S. Dimitriyev, S. E. Gonzalez, A. P. Cachine, S. Quinn, and E. A. Matsumoto, “Programming mechanics in knitted materials, stitch by stitch,” *Nature Communications* 2024 15:1, vol. 15, pp. 1–9, 2024.
- [7] P. B. Warren, R. C. Ball, and R. E. Goldstein, “Why clothes don’t fall apart: Tension transmission in staple yarns,” *Phys. Rev. Lett.*, vol. 120, p. 158001, 2018.
- [8] V. Sanchez, K. Mahadevan, G. Ohlson, M. A. Graule, M. C. Yuen, C. B. Teeple, J. C. Weaver, J. McCann, K. Bertoldi, and R. J. Wood, “3d knitting for pneumatic soft robotics,” *Advanced Functional Materials*, p. 2212541, 2023.
- [9] B. J. Collier and H. H. Epps, “Textile testing and analysis,” *Textile testing and analysis*, vol. 7, p. 374, 1999.
- [10] L. Tessmer, C. Dunlap, B. Sparrman, S. Kernizan, J. Laucks, and S. Tibbits, “Active textile tailoring,” *ACM SIGGRAPH 2019 Emerging Technologies, SIGGRAPH 2019*, 2019.
- [11] M. Popescu, “Knitcrete: Stay-in-place knitted formworks for complex concrete structures,” Ph.D. dissertation, ETH Zurich, 2019.
- [12] K. Mahadevan, M. C. Yuen, V. Sanchez, R. J. Wood, and K. Bertoldi, *Knitting multistability*, 2024. arXiv: 2410.14810 [cond-mat.soft].
- [13] X. Ding, V. Sanchez, K. Bertoldi, and C. H. Rycroft, “Unravelling the mechanics of knitted fabrics through hierarchical geometric representation,” *Proceedings of the Royal Society A*, vol. 480, 2024.
- [14] P. Wadekar, V. Perumal, G. Dion, A. Kontsos, and D. Breen, “An optimized yarn-level geometric model for finite element analysis of weft-knitted fabrics,” *Computer Aided Geometric Design*, vol. 80, p. 101883, 2020.
- [15] G. Sperl, R. M. Sánchez-Banderas, M. Li, C. Wojtan, and M. A. Otaduy, “Estimation of yarn-level simulation models for production fabrics,” *ACM Transactions on Graphics (TOG)*, vol. 41, pp. 1–15, 2022.
- [16] T. D. Dinh, O. Weeger, S. Kaijima, and S.-K. Yeung, “Prediction of mechanical properties of knitted fabrics under tensile and shear loading: Mesoscale analysis using representative unit cells and its validation,” *Composites Part B: Engineering*, vol. 148, pp. 81–92, 2018.
- [17] H. Hong, M. De Araujo, R. Fangueiro, and O. Ciobanu, “Theoretical analysis of load-extension properties of plain weft knits made from high performance yarns for composite reinforcement,” *Textile research journal*, vol. 72, pp. 991–996, 2002.
- [18] G. Sperl, R. Narain, and C. Wojtan, “Homogenized yarn-level cloth,” *ACM Transactions on Graphics*, vol. 39, 2020.
- [19] J. M. Kaldor, D. L. James, and S. Marschner, “Simulating knitted cloth at the yarn level,” in *ACM SIGGRAPH 2008 Papers*, ser. SIGGRAPH ’08, Los Angeles, California: Association for Computing Machinery, 2008, ISBN: 9781450301121.
- [20] J. M. Kaldor, D. L. James, and S. Marschner, “Efficient yarn-based cloth with adaptive contact linearization,” in *ACM SIGGRAPH 2010 Papers*, ser. SIGGRAPH ’10, Los Angeles, California: Association for Computing Machinery, 2010, ISBN: 9781450302104.
- [21] G. Cirio, J. Lopez-Moreno, and M. A. Otaduy, “Yarn-level cloth simulation with sliding persistent contacts,” *IEEE Transactions on Visualization and Computer Graphics*, vol. 23, pp. 1152–1162, 2017.
- [22] S. Huang and L. Huang, “Clo3d-based 3d virtual fitting technology of down jacket and simulation research on dynamic effect of cloth,” *Wireless Communications and Mobile Computing*, vol. 2022, p. 5835026, 2022.
- [23] P. J. McKee, A. C. Sokolow, J. H. Yu, L. L. Long, and E. D. Wetzel, “Finite element simulation of ballistic impact on single jersey knit fabric,” *Composite Structures*, vol. 162, pp. 98–107, 2017.
- [24] P. Grandgeorge, C. Baek, H. Singh, P. Johanns, T. G. Sano, A. Flynn, J. H. Maddocks, and P. M. Reis, “Mechanics of two filaments in tight orthogonal contact,” in *Proceedings of the National Academy of Sciences of the United States of America*, vol. 118, National Academy of Sciences, 2021, e2021684118.
- [25] C. Baek, P. Johanns, T. G. Sano, P. Grandgeorge, and P. M. Reis, “Finite element modeling of tight elastic knots,” *Journal of Applied Mechanics, Transactions ASME*, vol. 88, 2021.
- [26] S. Poincloux, M. Adda-Bedia, and F. Lechenault, “Geometry and elasticity of a knitted fabric,” *Physical Review X*, vol. 8, p. 021075, 2018.
- [27] J. Abel, J. Luntz, and D. Brei, “A two-dimensional analytical model and experimental validation of garter stitch knitted shape memory alloy actuator architecture,” *Smart Materials and Structures*, vol. 21, p. 085011, 2012.



- [28] O. Weeger, A. H. Sakhaei, Y. Y. Tan, Y. H. Quek, T. L. Lee, S.-K. Yeung, S. Kaijima, and M. L. Dunn, "Non-linear multi-scale modelling, simulation and validation of 3d knitted textiles," *Applied Composite Materials*, vol. 25, pp. 797–810, 2018.
- [29] S. Fillep, J. Mergheim, and P. Steinmann, "Towards an efficient two-scale approach to model technical textiles," *Computational Mechanics*, vol. 59, pp. 385–401, 2017.
- [30] M. El Messiry and E. Eltahan, "Analysis of the transverse compressive behavior of cotton yarns and fabrics," *Journal of Industrial Textiles*, vol. 53, p. 15 280 837 231 176 859, 2023.
- [31] L. Mullins, "Softening of rubber by deformation," *Rubber chemistry and technology*, vol. 42, pp. 339–362, 1969.
- [32] K. Crane, *A Simple Parametric Model of Plain-Knit Yarns*, online, 2023.
- [33] M. Smith, *ABAQUS/Standard User's Manual, Version 6.14*. Dassault Systemes Simulia Corp, 2014.
- [34] G. A. Holzapfel, T. C. Gasser, and R. W. Ogden, "A new constitutive framework for arterial wall mechanics and a comparative study of material models," *Journal of elasticity and the physical science of solids*, vol. 61, pp. 1–48, 2000.
- [35] C. Audet, S. Le Digabel, V. Rochon Montplaisir, and C. Tribes, "Algorithm 1027: NOMAD version 4: Nonlinear optimization with the MADS algorithm," *ACM Transactions on Mathematical Software*, vol. 48, 35:1–35:22, 2022.
- [36] Y. Xiong and X. Tao, "Compression garments for medical therapy and sports," *Polymers*, vol. 10, p. 663, 2018.
- [37] R. Granberry, K. Eschen, B. Holschuh, and J. Abel, "Functionally graded knitted actuators with niti-based shape memory alloys for topographically self-fitting wearables," *Advanced materials technologies*, vol. 4, p. 1 900 548, 2019.
- [38] K. Eschen, J. Abel, R. Granberry, and B. Holschuh, "Active-contracting variable-stiffness fabrics for self-fitting wearables," in *Smart Materials, Adaptive Structures and Intelligent Systems*, American Society of Mechanical Engineers, vol. 51944, 2018, V001T04A002.
- [39] F. Connolly, D. A. Wagner, C. J. Walsh, and K. Bertoldi, "Sew-free anisotropic textile composites for rapid design and manufacturing of soft wearable robots," *Extreme Mechanics Letters*, vol. 27, pp. 52–58, 2019.
- [40] K. Singal, M. S. Dimitriyev, S. E. Gonzalez, A. P. Cachine, S. Quinn, and E. A. Matsumoto, "Programming mechanics in knitted materials, stitch by stitch," *Nature Communications*, vol. 15, p. 2622, 2024.
- [41] S. Gore, R. Laing, C. Wilson, D. Carr, and B. Niven, "Standardizing a pre-treatment cleaning procedure and effects of application on apparel fabrics," *Textile research journal*, vol. 76, pp. 455–464, 2006.
- [42] K. Crane, *A Simple Parametric Model of Plain-Knit Yarns*, online, 2023.
- [43] H. Ding, W. Chen, and L. Zhang, *Elasticity of transversely isotropic materials*. Springer Science & Business Media, 2006, vol. 126.